

Electrically Pumped Microring Parity-Time-Symmetric Lasers

This article presents the design and implementation of nanoscale electrically pumped lasers based on microring resonators obeying parity-time symmetry, offering ideal properties for active nanophotonic applications.

By William E. Hayenga[®], Hipolito Garcia-Gracia, Enrique Sanchez Cristobal, Midya Parto, Hossein Hodaei, Patrick LiKamWa, Demetrios N. Christodoulides[®], and Mercedeh Khajavikhan

ABSTRACT | Microscale and nanoscale electrically pumped lasers are expected to play an indispensable role in future photonic integrated circuits. Small footprint, low threshold, high efficiency, and large side-mode suppression ratio (SMSR) are among the most important characteristics that such on-chip emitters should exhibit—allowing for large-scale integrability, low energy consumption, and stable output power. Microring resonators are one of the main contenders for the realization of such compact light sources. However, the use of microring laser cavities has been so far hindered by their tendency

to operate in multiple modes. Quite recently, several studies have shown that notions from parity-time (PT)-symmetry and non-Hermitian physics can be utilized to effectively enforce single-mode operation in semiconductor microring laser arrangements. However, as of now, most works in this area were mainly devoted to the proof of concept demonstrations, while the feasibility of practical implementation has remained largely unexplored. In this article, we demonstrate the first regrowth free, electrically pumped microscale PT-symmetric laser. Our results can pave the way toward the utilization of exceptional points in more diverse applications ranging from on-chip light sources and modulators to laser beam steering systems and active sensors.

KEYWORDS | Optical waveguides; ring lasers; semiconductor lasers.

Manuscript received January 31, 2019; revised August 1, 2019; accepted August 4, 2019. Date of publication September 11, 2019; date of current version April 28, 2020. This work was supported in part by the Office of Naval Research (ONR) under Grant N00014-16-1-2640, Grant N00014-18-1-2347, and Grant N00014-19-1-2052, in part by the National Science Foundation (NSF) under Grant ECCS 1454531, Grant DMR-1420620, Grant ECCS 1757025, and Grant CBET 1805200, in part by the Air Force Office of Scientific Research (AFOSR) under Grant FA9550-14-1-0037, in part by Army Research Office (ARO) under Grant W911NF-16-1-0013 and Grant W911NF-17-1-0481, in part by the U.S.-Israel Binational Science Foundation (BSF) under Grant 2016381, in part by The Defense Advanced Research Projects Agency (DARPA) under Grant D18AP00058, Grant HR00111820042, and Grant HR00111820038, and in part by the Qatar National Research Fund under Grant NPRP 9-020-1-006. (Corresponding author: Mercedeh Khajavikhan.)

- W. E. Hayenga, E. Sanchez Cristobal, M. Parto, P. LiKamWa, and D. N. Christodoulides are with CREOL, The College of Optics and Photonics, University of Central Florida, Orlando, FL 32816 USA (e-mail: whayenga34@knights.ucf.edu).
- **H. Garcia-Gracia** was with CREOL, The College of Optics and Photonics, University of Central Florida, Orlando, FL 32816 USA. He is now with Grupo 4S, Monterrey 66230, Mexico.
- H. Hodaei was with CREOL, The College of Optics and Photonics, University of Central Florida, Orlando, FL 32816 USA. He is now with Infinera Corporation, Sunnyvale, CA 94089 USA.
- M. Khajavikhan was with The College of Optics and Photonics, University of Central Florida, Orlando, FL 32816 USA. She is now with the Ming Hsieh Department of Electrical and Computer Engineering, University of Southern California, Los Angeles, CA 90089 USA (e-mail: mercedeh@creol.ucf.edu; khajavik@usc.edu).

Digital Object Identifier 10.1109/JPROC.2019.2935901

I. INTRODUCTION

In the past few decades, extensive research has been conducted toward the development of on-chip electrically injected lasers. For many applications, low threshold, high efficiency, small footprint, and large side-mode suppression ratio (SMSR) are among the most desired properties that such light sources should possess [1], [2]. To some extent, these attributes have been successfully attained in a number of semiconductor laser arrangements, such as distributed Bragg reflector (DBR) [3] systems, distributed feedback (DFB) [4], and vertical-cavity surface-emitting lasers (VCSELs) [5], [6]. In all these devices, frequency selectivity is enforced through the use of intracavity dispersive elements. However, there is an ever-growing demand for improving the performance of lasers, not only in regard to size, emission directionality,

0018-9219 © 2019 IEEE. Personal use is permitted, but republication/redistribution requires IEEE permission. See https://www.ieee.org/publications/rights/index.html for more information.

and ease of fabrication. In this respect, the vertical emission associated with VCSELs makes their use in planar on-chip settings challenging, while the fabrication process of record performance DFB lasers, in general, involves one or two regrowth steps. Consequently, the realization of a microscale, single-mode, side-coupled, and regrowth-free laser arrangement still remains elusive.

II. PARITY-TIME-SYMMETRY IN OPTICS AND PARITY-TIME SYMMETRIC MICRORING LASERS

First introduced in the context of quantum field theory [7], [8], the concept of PT-symmetry recently gained considerable attention in optics [9]-[21]. A photonic structure respects PT-symmetry, provided its corresponding wave-Hamiltonian commutes with the PT operator. In this regard, a necessary, albeit not sufficient, condition for an optical system to be PT-symmetric is that the complex refractive-index distribution follows the relationship $n^*(-r) = n(r)$. A direct outcome of non-Hermiticity is the emergence of exceptional points (EPs), also known as PT-symmetry breaking points in the parameter space. Such non-Hermitian degeneracies have been shown to lead to a number of new and counter-intuitive phenomena in the realm of optics. These include, for example, loss-induced transparency [10], [11], unidirectional invisibility and band merging [12]-[16], and loss-induced suppression and revival of lasing [17], [18]. In addition, laser-mode management [19]-[25], lasing/antilasing behavior in a single cavity [26], spawning rings of EPs in photonic crystals [27], chiral-state conversion via EP encirclements [28], [29], and enhanced sensitivity [30]-[32] have also been demonstrated in such configurations. Extensive review articles concerning these topics can be found in [33]-[36].

Microring resonators are one of the most promising candidates for on-chip laser applications. To start with, they characteristically exhibit high-quality factors and large mode confinement [37]. Moreover, by virtue of their geometry, they can be readily coupled in on-chip photonic circuits through appropriately designed bus waveguides. However, despite their relatively large free spectral range, even small microrings support multiple longitudinal modes with comparable quality factors within the broad line shape of most semiconductor gain systems. Even though the spectral curvature of this line shape function offers some level of mode discrimination between various longitudinal modes, such lasers tend to easily become multimoded as the pump increases above the threshold value. Therefore, additional mechanisms should be employed in order to guarantee high-fidelity single-mode lasing in these configurations.

Previously, we demonstrated how using the difference between the threshold of PT-symmetry breaking for various longitudinal modes can result in high-fidelity single-mode operation in microring lasers under optical

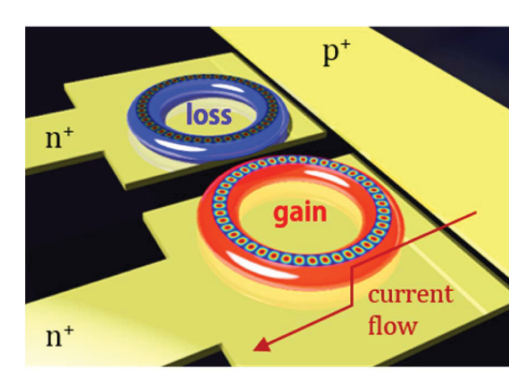


Fig. 1. Schematic of an electrically injected PT-symmetric microring laser arrangement.

pumping. In this article, we provide the first realization of a microscale, regrowth-free, electrically pumped single-mode PT-symmetric laser system on a III–V semiconductor platform.

Fig. 1(a) depicts a schematic of an electrically pumped PT-symmetric microring laser. This structure is comprised of two identical cavities, one subject to gain, while the other one kept lossy. Under such conditions, the temporal evolution of the electric field envelopes within these cavities is to the first order described by the following coupled equations:

$$i\frac{dA_1}{dt} + i\gamma_1 A_1 + KA_2 = 0$$

$$i\frac{dA_2}{dt} + i\gamma_2 A_2 + KA_1 = 0$$
(1)

where A_1 and A_2 are the associated wave amplitudes in the cavities with loss and gain respectively, γ_1 and γ_2 represent the net linear gain/loss coefficient, and K is the temporal coupling coefficient between the microrings. Using this, it is now clear that the wave-Hamiltonian describing (1), after a gauge transformation, respects PT symmetry [20]. Even though the above-mentioned simplified formalism can capture some of the main features of this lasing system, a more detailed description concerning the nonlinearities of gain and loss is needed for a more thorough analysis. Such an analysis can be found in [38].

When two identical resonators with the same levels of gain or loss ($\gamma_1=\gamma_2$) are placed next to one another, the degeneracy between their respective modes is broken. The frequency splitting $\delta\omega$ of the resulting supermode doublets is directly proportional to the coupling coefficient, i.e., $\delta\omega=2$ K. The resulting eigenfrequencies of such an active system can, in general, be complex, and their imaginary part describes amplification or attenuation. Meanwhile, in PT-symmetric arrangements (where there is a contrast between the gain of the two resonators), the relationship between eigenfrequencies and coupling is by nature different, as indicated by $\delta\omega=2(K^2-1/4(\gamma_1-\gamma_2)^2)^{1/2}$. Consequently, in this arrangement, the longitudinal modes, whose gain–loss contrast $(\delta\gamma=1/2|\gamma_1-\gamma_2|)$ remains below the coupling coeffi-

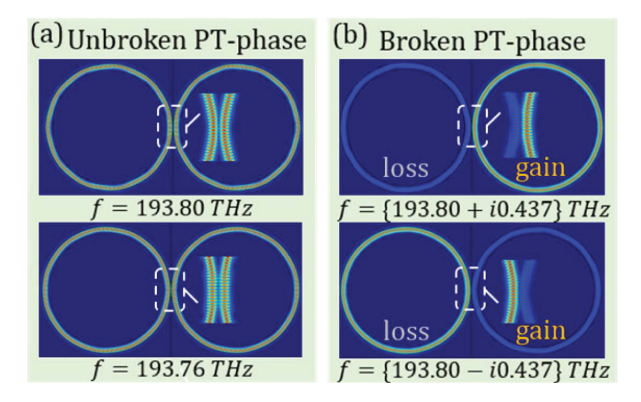


Fig. 2. FEM simulations of coupled metallic microring lasers.

(a) Results of the electromagnetic modes operating in the unbroken PT-phase. (b) Broken phase regime, where the gain-loss contrast exceeds the coupling strength, and hence, the corresponding modes tend to reside in either the active or lossy ring.

cient K, undergo bounded neutral oscillations. However, as soon as $\delta\gamma$ exceeds K, a conjugate pair of lasing and decaying modes emerges. Clearly, judicious placement of this PT threshold will allow for a complete suppression of all nonbroken mode pairs in favor of a single amplified mode associated with the aforementioned conjugate pair. Furthermore, it has been shown that this strategy can enhance the single-mode operation by a factor of $(g_1+g_2)^{1/2}/(g_1-g_2)^{1/2}$, where g_1 and g_2 are the available gain associated with the first and second modes that are closest to the peak of the line shape [20], [39].

A. Theoretical Estimation of the Temporal Coupling Between the Rings

The rings under study have widths of 1 μ m and outer radii of 10 μ m (expected free spectral range of \sim 10 nm). The separation between them is designed to be 100 nm, translating to a coupling strength of \sim 60 GHz. The modes of these structures, centered at a wavelength of 1550 nm, simulated using finite-element methods (FEMs), are shown in Fig. 2(a) and (b) when the system is below and above the PT-symmetry breaking threshold, respectively. In this regard, when the gain/loss contrast is small, the two whispering gallery supermodes reside equally in both cavities [Fig. 2(a)]. On the contrary, when the gain/loss difference exceeds the coupling strength between the two rings, the PT-symmetry is broken [Fig. 2(b)], thus enforcing the single-mode operation. To achieve this, the device should be biased such that only the fundamental longitudinal mode (with the highest gain) operates in the PT-symmetry breaking regime, while the rest of the resonances are kept below their respective phase transition points. In this case, higher order longitudinal modes are effectively suppressed since they are subject to a considerable amount of loss associated with the unpumped cavity [20].

To calculate the temporal coupling coefficient between the rings, we first evaluated the effective coupling between the TE modes of the cross-sectional waveguides of the structure. Fig. 3 shows these cross-sectional waveguides, where the simulated odd [Fig. 3(a)] and even [Fig. 3(b)] supermodes are computed using COMSOL Multiphysics' mode solver. The geometry in this simulation is composed of InGaAs core layers with a refractive index of 3.44, upper and lower cladding layers of InP with refractive index 3.17, while the whole geometry is surrounded by benzocyclobutene (BCB) corresponding to a refractive index of 1.54. Moreover, the sides of the rings are covered by a 100-nm-thick Si₃N₄ buffer layer of refractive index 2.00. The dependence of the coupling in this structure on the separation distance between the rings is estimated to be $\kappa(x) = \kappa_0 e^{-x/x_0}$, where x denotes the separation measured in micrometers and $x_0 = 13.8\mu\text{m}$. The effective coupling between the rings can now be calculated using

$$\kappa L_e = \int_{-y_0}^{y_0} \kappa(y) \, dy \tag{2}$$

where y is the propagation distance along the circumference of the rings. In our simulated structure, the effective coupling is estimated to be $\kappa L_e \approx 5.28 \times 10^{-2}$. Now, the corresponding temporal coupling between the rings can be estimated as

$$K = \frac{1}{2\pi} \times \frac{c}{2\pi R n_e} \kappa L_e \approx 1.3 \times 10^{10} \text{s}^{-1}$$
 (3)

where n_e is the mode effective index, while R is the radius of the microring resonator. In practice, however, we generally expect a greater coupling than what this simplified model predicts. This can be attributed to the following three factors.

- 1) Near-field enhancement mediated by side-wall roughness.
- 2) Imperfect etching which leads to a reminiscent layer of InP unetched, as shown in Fig. 4(a). This will lead to an increased coupling between the rings, due to less confinement of the fields inside cross-sectional waveguides [Fig. 4(b)]. According to our simulations, this will lead to a factor of $\sim \times 3$ enhancement in K.
- 3) The decrease in the refractive index of the core gain medium, as predicted by a positive linewidth

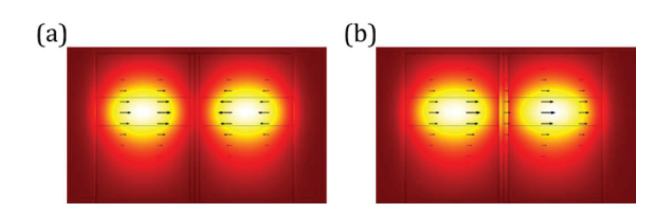


Fig. 3. TE mode coupling in the cross-sectional waveguides of the rings. Electric field intensity $|E|^2$ associated with the (a) odd and (b) even TE supermodes of the cross-sectional waveguides of the rings.

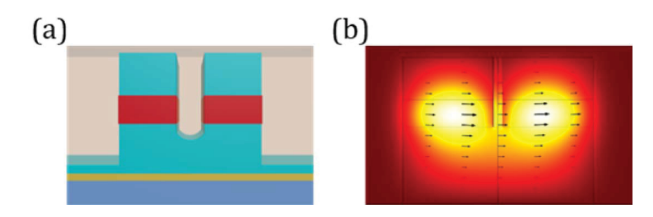


Fig. 4. Enhanced mode coupling between two rings due to an imperfect etching. (a) Schematic representing the cross-sectional view of the coupling region between two rings, where the InP layer in the middle is not completely etched to the bottom. (b) Electric field intensity associated with the even TE supermode of this coupled waveguide configuration. Notice that the leakage of the electric field in this case is considerably higher than in Fig. 3, resulting in a higher coupling coefficient between the rings.

enhancement factor. This can be understood from the field evolution equation in a semiconductor ring laser

$$\frac{dE}{dt} = \frac{1}{2} \left[-\gamma + \sigma \left(N - 1 \right) \right] \left(1 - i\alpha_H \right) E \tag{4}$$

where E is the electric field amplitude, γ is inversely proportional to the photon lifetime in the ring, σ is related to the gain coefficient, and N represents the normalized carrier density. The linewidth enhancement factor is denoted here as α_H , which is a positive quantity.

As a result, the change in the real part of the refractive index can be obtained as

$$\Delta n = -\frac{\sigma(N-1)\alpha_H n_g}{2\omega_0} \tag{5}$$

where ω_0 is the resonance frequency of the unpumped cavity. In our simulations, we considered the change in the coupling due to a decrease of 2% in the refractive index of the gain medium. In this case, the calculated temporal coupling will increase to $K\approx 4.5\times 10^{10}\,\mathrm{s^{-1}}$ due to less confinement of the electromagnetic fields in the cross-sectional waveguides of the rings. In our experiments, we verified this effect by increasing the pump currents (while both rings were pumped equally) and observed a rise in the measured coupling levels from $K\approx 7.5\times 10^{10}~\mathrm{s^{-1}}$ to $K\approx 8.5\times 10^{10}~\mathrm{s^{-1}}$.

III. FABRICATION AND CHARACTERIZATION

A. Fabrication of Electrically Pumped Parity-Time Symmetric Microring Lasers

The platform for our devices is based on an InGaAs/InP structure grown on an undoped InP substrate by molecular beam epitaxy (MBE). The epitaxial layers were grown by OEpic Semiconductors Inc. The gain region consists of 300 nm of undoped bulk InGaAs sandwiched

between an n-doped 470-nm InP cladding and a p-doped 850-nm InP layer. Highly doped n-InGaAs and p-InGaAsP form the n- and p-contact layers. Fig. 5 displays the detailed wafer structure. The materials and dopings are appropriately labeled.

The microring resonators are fabricated using standard nanofabrication techniques. The microrings are patterned into FOx-16 Flowable Oxide (e-beam resist) by high-resolution e-beam lithography [Fig. 6(a)] and then transferred to the wafer by a reactive ion etching (RIE) process using a H₂:CH₄:Ar (40:4:20 sccm) chemistry [Fig. 6(b)]. The polymer byproducts of the RIE process are subsequently removed from the sample with oxygen plasma cleaning. Next, a 100-nm layer of silicon nitride (Si₃N₄) is deposited on our structure by plasma-enhanced chemical vapor deposition (PECVD) [Fig. 6(c)]. The area for the p-contact is defined by photolithography, and the underlying highly doped p⁺ InGaAsP layer is accessed through dry etching of the Si₃N₄ layer and wet etching of the remaining InP layer in an HCl:H₃PO₄ (1:1) solution. The p-contact is formed by thermal evaporation of Ti/Au (10/300 nm) and photoresist liftoff in RR41 remover [Fig. 6(d)]. We spin a layer of BCB polymer in order to produce a planarized surface to deposit the n-contact, as well as to electrically insulate the n- and p-contact layers. The BCB polymer is etched in O2:CF4 plasma (10:5 sccm) until the FOx-16 resist on the top of the microring resonators is uncovered, which is ultimately wet etched with buffered oxide etch (BOE) [Fig. 6(e)]. The n-contact is formed by photolithographic patterning, thermal evaporation of nickel (5 nm), eutectic goldgermanium (150 nm), and gold (400 nm), and photoresist liftoff [Fig. 6(f)]. Fig. 7(a) and (b) shows the scanning electron microscope (SEM) images of the structure after dry etching and the p-contact deposition, respectively; on the other hand, Fig. 7(c) shows a microscopic image of the structure after defining the n⁺ contacts. The sample is then subjected to a rapid thermal annealing process at 430 °C for 30 s to fuse the metals and reduce the resistance of the contacts. Finally, the sample is mounted on a TO-8 header and wire-bonded for testing. The light is then collected

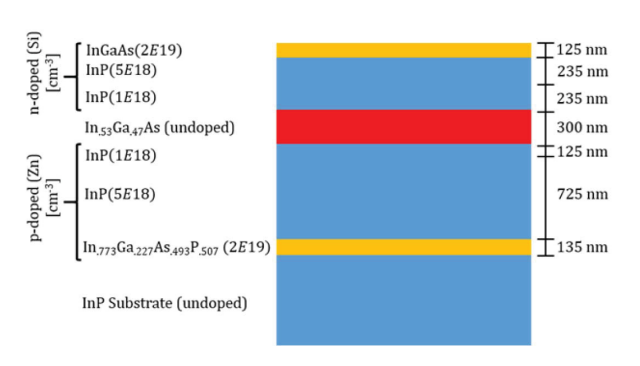


Fig. 5. Detailed wafer schematic. The wafer is epitaxially grown. The material thickness and parameters are detailed in the illustration.

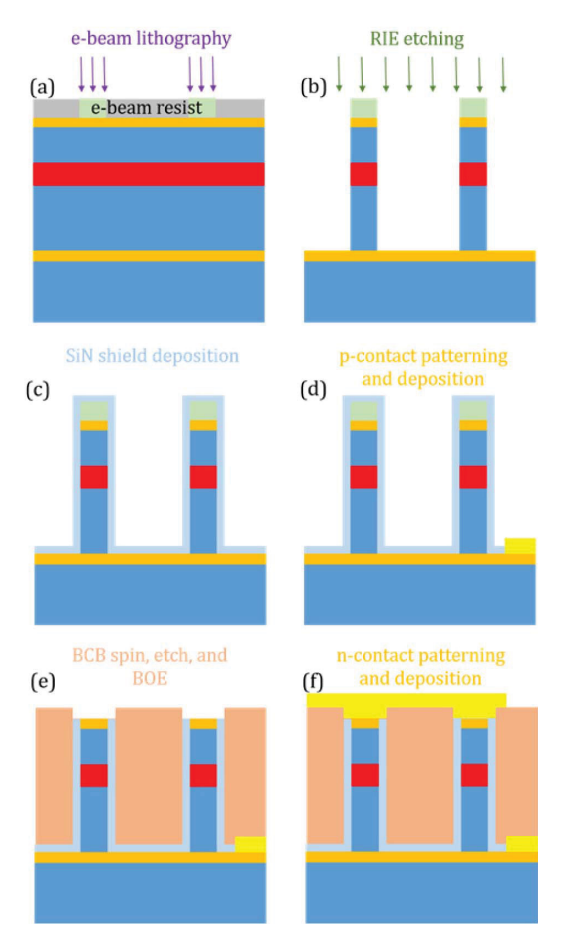


Fig. 6. Fabrication process of the PT-symmetric microring laser. (a) FOx-16 negative tone resist is spun onto the wafer. The pattern is defined with e-beam lithography. (b) Cavities are formed with RIE. (c) PECVD to create a 100-nm Si₃N₄ dielectric layer on the sample. (d) p-contact (10/300 nm Ti/Au) is deposited with a thermal evaporator. (e) BCB is spun onto the sample, baked, and etched away until the midway point of the FOx-16 pillar. BOE is used to remove this pillar. (f) n-contact (5/150/400 nm Ni/Au-Ge eutectic/Au) is deposited via thermal evaporation.

from the backside of the sample through a hole inscribed in the center of the header when testing.

B. Characterization Setup

For device characterization, a microelectroluminescence (μ -EL) setup is employed to collect the emission spectrum, output power, and mode profile. Fig. 8 depicts the schematic of the μ -EL characterization setup. A 50X microscope objective with a numerical aperture of 0.42 is used to collect the emission from the PT-symmetric lasers. This emission is either imaged into a spectrometer (Princeton Instruments Acton SP2300) with an attached liquid nitrogen linear array detector (Princeton Instruments OMA V) for spectral inspection or to an IR camera (Xeva-1.7-320) to capture the intensity profile. The kinematic mirror is to select one path or the other. To locate the patterns, the sample surface is imaged by illuminating it

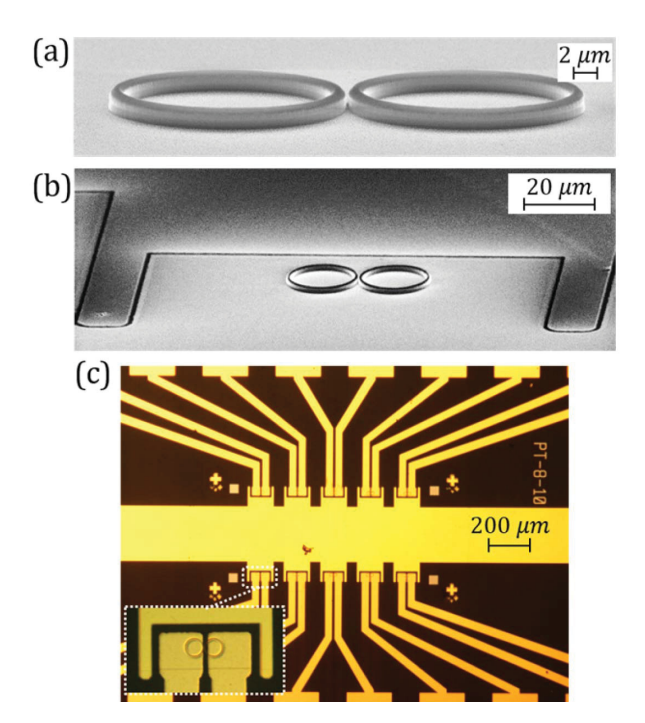


Fig. 7. Scanning electron and microscope images associated with the electrically pumped PT-symmetric laser. An SEM image of (a) patterned rings after RIE etching and (b) of the sample after defining the p+ contact. (c) Microscope image of the structure after forming the n+ contacts. Inset: zoomed-in image of the rings.

with a broadband IR source (Amonics) in a confocal microscope configuration. The sample is inserted into a continuous-flow microscopy cryostat (Janis ST-500) equipped with electrical feedthroughs and cooled with liquid nitrogen to a temperature of 77 K. The lasers are electrically pumped using a current driver (ILX Lightwave LDP-3840B) generating pulse widths of 116 ns at a repetition rate of 50 kHz. The laser diode is connected to

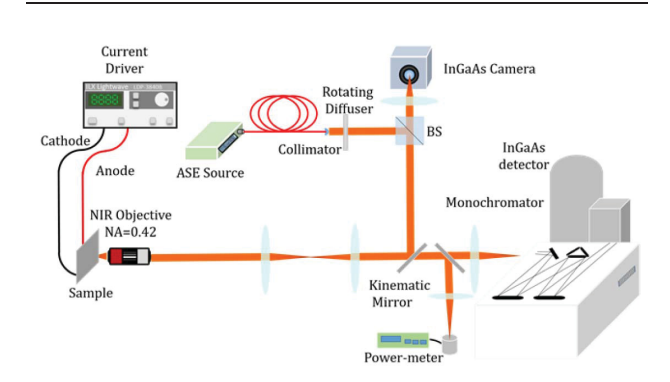


Fig. 8. μ -EL characterization setup. The sample is pumped with a pulsed current driver. The emission is collected by a 50X objective and directed into a monochromotor with an attached InGaAs array detector or to an InGaAs camera or power meter. An ASE source is used in conjunction with a rotating diffuser for purposes of imaging the sample surface.

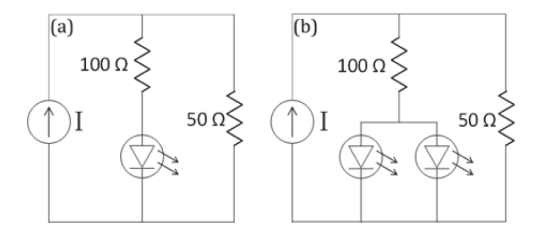


Fig. 9. Circuit schematic used for pulsed electrical injection (a) for a PT-symmetric laser and (b) when pumping both cavities in the double-ring arrangement. The circuit consists of a pulsed current driver and two parallel series, one with a $50-\Omega$ resistor and the other with a $100-\Omega$ resistor, and the laser diode. The average voltage is measured across the $100-\Omega$ resistor for current measurements.

the current source in series with a 100- Ω resistor. The average voltage across this resistor is measured with a voltmeter to obtain the average current and is then divided by the duty cycle to arrive at the equivalent continuous wave (CW) current. For proper pump shaping and finer current resolution, a circuit with only a 50- Ω resistor is connected in parallel to the laser diode and 100 Ω resistor [Fig. 9(a) and (b)]. Output power of the lasers was measured with an IR photodiode (Newport Model 818-IR). This too was divided by the duty cycle for an equivalent CW power. The reported power also factors in the losses

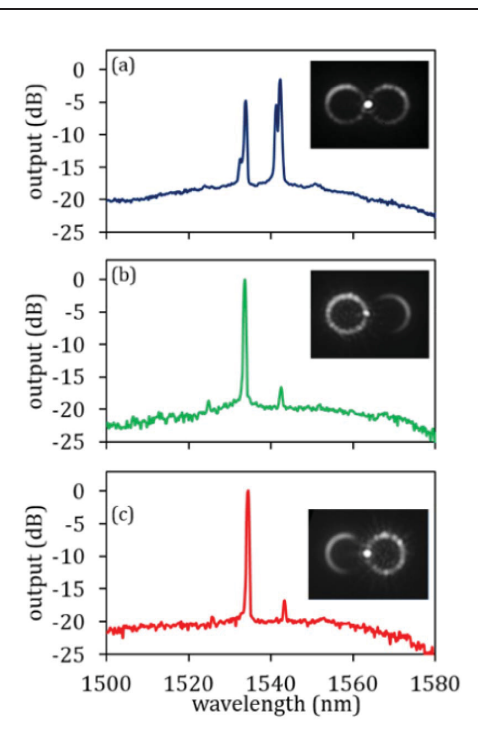


Fig. 10. Semilogarithmic single-shot spectra of the microring lasers. Semilogarithmic single-shot spectra taken at an injection current of 1.8 mA when (a) both cavities are pumped, and when only the (b) left, or (c) right ring is subject to gain. The splitting in the resonance frequency of the longitudinal modes is observed when both cavities are equally pumped in (a). When the PT-symmetry is broken, a single mode with an SMSR of \sim 18 dB emerges at the center of the splitting, as observed in (a).

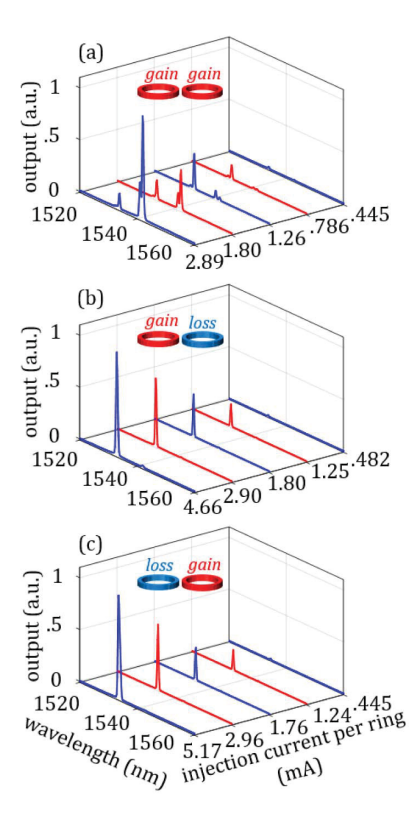


Fig. 11. Spectral evolution when (a) both cavities are pumped, and when only the (b) left or (c) right ring is injected with current. The spectral evolution shows the onset of higher order modes as the current increases (a). When operating in the broken PT-symmetric regime [(b) and (c)], the device remains single-moded at currents greater than ten times the threshold.

associated with the characterization setup, such as propagation through substrate, cryostat glass reflection, and optical elements such as objective, lenses, and filters.

IV. EXPERIMENT

The experimental results regarding the active coupled ring arrangement under different injection conditions are presented in Figs. 10 and 11. We started by pumping both cavities with almost equal currents. The semilogarithmic spectrum in Fig. 10(a) clearly shows that the resonance frequency associated with each longitudinal mode splits into two lines (separated by ~ 1 nm), due to the coupling between the rings. In this regime of operation, the spectral evolution of the device is depicted in Fig. 11(a) where the measurement results are reported from near threshold to more than six times above the threshold current. When both resonators are pumped, this laser system always operates in a multimode fashion. Next, a gauged PT-symmetric arrangement is realized by injecting different current levels into the two cavities. In this latter scenario, the gain/loss contrast is judiciously adjusted in order to enforce singlemode operation. This leads to a measured SMSR of \sim 18 dB when the PT-symmetric laser is set to four times the threshold current [Fig. 10(b)]. The spectral evolution of the laser in the gauged PT-symmetric configuration

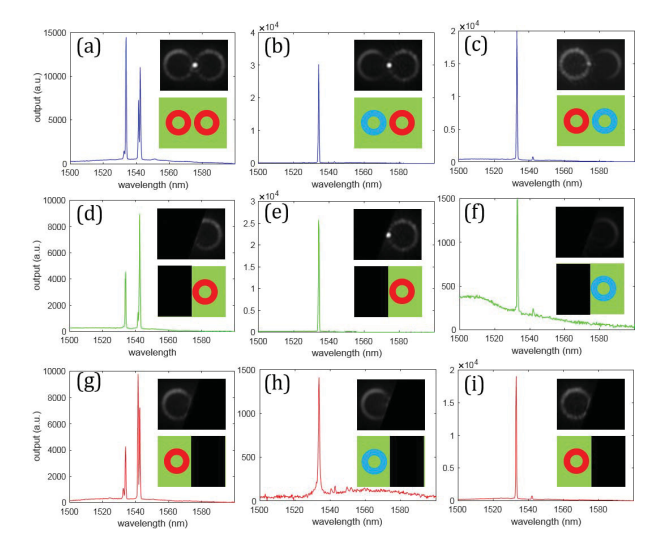


Fig. 12. Experimental results demonstrating the coupling between the rings. A knife edge is utilized to spatially filter the light scattered from a single ring in the arrangement. The top inset shows the recorded emission profile. The bottom inset is used to clarify which ring is being spatially filtered by the knife edge. The pumped and unpumped rings are red and blue, respectively. (a), (d), and (g) When both rings are pumped, splitting of the longitudinal modes is observed, regardless of which ring's emission is spatially filtered by the knife edge. (b), (e), and (h) Right ring and (c), (f), and (i) left ring is injected with current, respectively.

is presented in Fig. 11(b). In this case, the laser faithfully remains single moded even when pumped at ten times the threshold current. Similar results are obtained when the current is switched between the two cavities [Figs. 10(c) and 11(c)]. The fact that the lasing frequencies shown in Fig. 10(b) and (c) are identical further confirms that the observed behavior is indeed associated with a coupled non-Hermitian system. The intensity profiles in the two cavities presented in the insets of Fig. 10(b) and (c) show that under PT-symmetric conditions the mode almost exclusively resides in the cavity subjected to gain, while most of the cavity subjected to gain, while most of the emission from the lossy cavity is associated with photoluminescence (PL). On the other hand, in the evenly pumped configuration, both cavities appear to equally participate in the lasing process [Fig. 10(a)]. The selection of the longitudinal mode at the shorter wavelength could be because of the red shift of the gain spectra in the evenly pumped scheme.

A. Ring Emission Comparisons

In order to confirm coupling between the two rings, we observed the associated spectrum of the rings under varying pumping conditions. A knife edge is utilized to spatially filter the light scattered from a single ring in the arrangement. When both rings are pumped [Fig. 12(a), (d), and (g)], splitting of the longitudinal modes is observed in the spectrum, regardless of whichring's emission is spatially filtered by the knife edge-demonstrating that pair of microrings

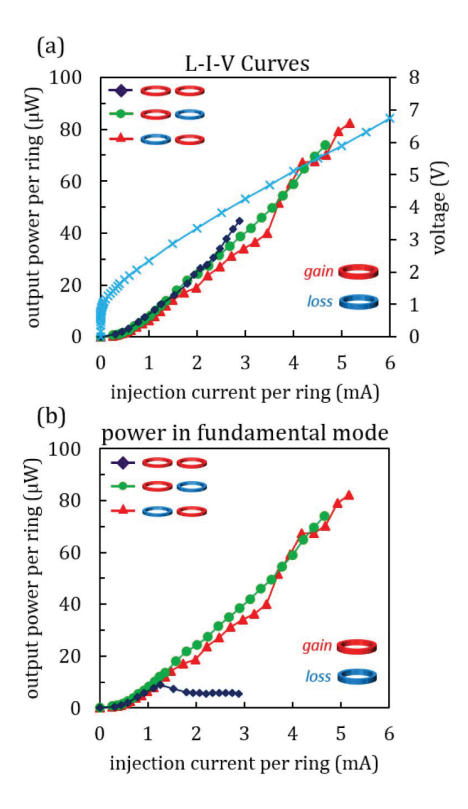


Fig. 13. Light-current-voltage characteristics. (a) Light-current curves obtained when both rings are equally pumped and under PT-symmetric conditions corresponding to scenarios shown in Fig. 11. The light blue crosses denote the I-V curve. (b) Spectrally resolved plot shows the onset of higher order modes in the doubly pumped ring configuration. The PT-symmetric arrangement inhibits the growth of unwanted parasitic modes while exhibiting nearly the same slope efficiency.

are indeed coupled. Furthermore, when a single ring is injected with current, it is observed that the light is primarily being emitted from the pumped cavity, as expected [Fig. 12 (b), (e), and (h) and (c), (f), and (i)].

B. Light-Current-Voltage Curves

An important aspect of lasing in PT-symmetric systems is the fact that, perhaps in a counter-intuitive way, the loss does not affect the slope efficiency of the laser. This is because above the PT-symmetry breaking point, non-Hermiticity effectively decouples the two cavities involved. Hence, the broken mode that is residing in the pumped cavity remains entirely oblivious to the loss in the neighboring resonator. Fig. 13(a) shows the light-current (L-I) curve associated with different pumping scenarios (evenly pumped vs. PT-symmetric). Despite being coupled to a lossy element, the PT-symmetric laser exhibits a slope efficiency comparable to that obtained from the evenly pumped ringsonly this time, it is single moded. Fig. 13(b) displays the L-I curve for the output power of the fundamental mode, indicating a superior performance for the PT-symmetric arrangement in terms of power extracted per mode.

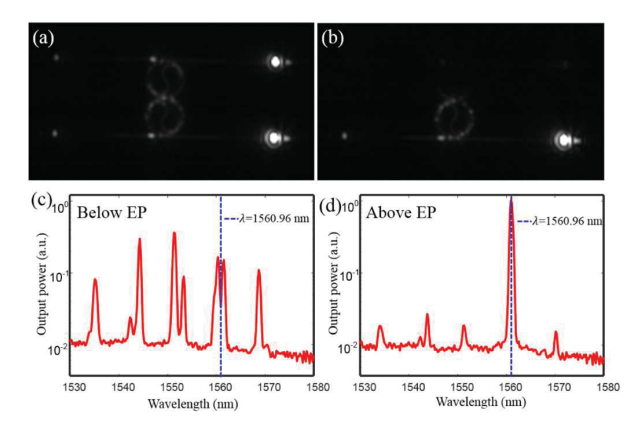


Fig. 14. Unidirectional PT-symmetric microring lasers. (a) and (b) Camera images from the coupled microcavities, bus waveguides, and outcoupling gratings (a) below and (b) above the PT-symmetric breaking point. (c) and (d) Corresponding spectra (log scale).

The current–voltage (I–V) characteristics of the PT-symmetric lasers were collected at a temperature of 77 K. A direct current driver (Keithley 224) was used as the source. A voltmeter was connected across the laser diode and the voltage was recorded for various injection currents [light-blue line in Fig. 13(a)]. The relatively large differential resistance (2076 Ω) is attributed to the slower hole mobility in the heavily p-doped InGaAsP layer to the p-contact.

C. Laser Coupling to a Bus Waveguide

For integrated photonic applications, it is imperative to collect the emission from the laser using a bus waveguide. It is also important to enforce unidirectional light propagation in the rings. These aspects have been previously studied in [40]. For example, it has been shown that including an S-shaped bend in the resonator will result in unidirectional lasing [40]. Fig. 14 shows the possibility of using a bus waveguide in optically pumped arrangements. The bus waveguide is equipped with second-order gratings to outcouple the light. The PT-symmetry and single-mode operation are fully preserved in the presence of symmetrically incorporated bus waveguides.

V. CONCLUSION

In conclusion, we reported the first demonstration of a PT-symmetric single-mode microscale on-chip electrically injected microring laser. Its regrowth-free fabrication process, small foot-print, low threshold (445 μ A), and large SMSR (\sim 18 dB) makes it an attractive light source for applications in photonic integrated circuits. The device demonstrated in this article is yet far from a practical laser for integrated photonics, but it certainly has the potential to be used in many applications where on-chip, single-mode lasers are needed. The realization of electrically pumped PT-symmetric lasers may pave the way toward using these systems as on chip sources in a variety of applications or in emerging areas of PT-symmetric sensors and gyroscopes.

REFERENCES

- D. A. B. Miller, "Device requirements for optical interconnects to silicon chips," *Proc. IEEE*, vol. 97, no. 7, pp. 1166–1185, Jul. 2009.
- [2] A. W. Fang, H. Park, O. Cohen, R. Jones, M. J. Paniccia, and J. E. Bowers, "Electrically pumped hybrid AlGaInAs-silicon evanescent laser," Opt. Express, vol. 14, no. 20, pp. 9203–9210, 2006.
- [3] F. K. Reinhart, R. A. Logan, and C. V. Shank, "GaAs-Al_xGa₁ - xAs injection lasers with distributed Bragg reflectors," Appl. Phys. Lett., vol. 27, p. 45, Sep. 1975.
- [4] M. Nakamura, A. Yariv, H. W. Yen, S. Somekh, and H. L. Garvin, "Optically pumped GaAs surface laser with corrugation feedback," *Appl. Phys. Lett.*, vol. 22, no. 10, pp. 515–516, 1973.
- [5] H. Soda, K.-I. Iga, C. Kitahara, and Y. Suematsu, "GalnAsP/InP surface emitting injection lasers," *Jpn. J. Appl. Phys.*, vol. 18, no. 12, pp. 2329–2330, 1979.
- [6] L. A. Coldren, S. W. Corzine, and M. L. Mashanovitch, *Diode Lasers and Photonic Integrated Circuits*. Hoboken, NJ, USA: Wiley, 2012.
- [7] C. M. Bender and S. Boettcher, "Real spectra in non-Hermitian Hamiltonians having PT symmetry," Phys. Rev. Lett., vol. 80, no. 24, p. 5243, 1998.
- [8] C. M. Bender, D. C. Brody, and H. F. Jones, "Complex extension of quantum mechanics," *Phys. Rev. Lett.*, vol. 89, Dec. 2002, Art. no. 270401.
- [9] K. G. Makris, R. El-Ganainy, D. N. Christodoulides, and Z. H. Musslimani, "Beam dynamics in PT symmetric optical lattices," *Phys. Rev. Lett.*, vol. 100, no. 10, 2008, Art. no. 103904.
- [10] A. Guo *et al.*, "Observation of PT-symmetry breaking in complex optical potentials," *Phys. Rev. Lett.*, vol. 103, po. 9, 2009. Art. po. 093902
- Lett., vol. 103, no. 9, 2009, Art. no. 093902.
 [11] C. E. Rüter, K. G. Makris, R. El-Ganainy,
 D. N. Christodoulides, M. Segev, and D. Kip,

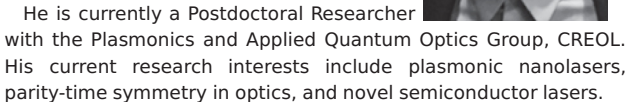
- "Observation of parity-time symmetry in optics," *Nature Phys.*, vol. 6, no. 3, pp. 192–195, 2010.
- [12] Z. Lin, H. Ramezani, T. Eichelkraut, T. Kottos, H. Cao, and D. N. Christodoulides, "Unidirectional invisibility induced by PT-symmetric periodic structures," *Phys. Rev. Lett.*, vol. 106, no. 21, 2011, Art. no. 213901.
- [13] A. Regensburger, C. Bersch, M.-A. Miri, G. Onishchukov, D. N. Christodoulides, and U. Peschel, "Parity-time synthetic photonic lattices," *Nature*, vol. 488, no. 7410, pp. 167–171, 2012.
- [14] L. Feng et al., "Experimental demonstration of a unidirectional reflectionless parity-time metamaterial at optical frequencies," *Nature Mater.*, vol. 12, no. 2, pp. 108–113, 2013.
- [15] B. Peng et al., "Parity-time-symmetric whispering-gallery microcavities," *Nature Phys.*, vol. 10, no. 5, pp. 394–398, 2014.
- [16] L. Chang et al., "Parity-time symmetry and variable optical isolation in active-passive-coupled microresonators," *Nature Photon.*, vol. 8, pp. 524–529, Jul. 2019.
- [17] M. Brandstetter et al., "Reversing the pump dependence of a laser at an exceptional point," Nature Commun., vol. 5, Jun. 2014, Art. no. 4034.
- [18] B. Peng et al., "Loss-induced suppression and revival of lasing," Science, vol. 346, no. 6207, pp. 328–332, 2014.
- [19] M.-A. Miri, P. LiKamWa, and D. N. Christodoulides, "Large area single-mode parity-time-symmetric laser amplifiers," Opt. Lett., vol. 37, pp. 764–766, Mar. 2012.
- [20] H. Hodaei, M.-A. Miri, M. Heinrich, D. N. Chrisodoulides, and M. Khajavikhan, "Parity-time-symmetric microring lasers," *Science*, vol. 346, pp. 975–978, Nov. 2014.
- [21] L. Feng, Z. J. Wong, R.-M. Ma, Y. Wang, and

- X. Zhang, "Single-mode laser by parity-time symmetry breaking," *Science*, vol. 346, pp. 972–975, Nov. 2014.
- [22] H. Hodaei et al., "Single mode lasing in transversely multi-moded PT-symmetric microring resonators," Laser Photon. Rev., vol. 10, pp. 494–499, May 2016.
- [23] Z. Gao, S. T. Fryslie, B. J. Thompson, P. S. Carney, and K. D. Choquette, "Parity-time symmetry in coherently coupled vertical cavity laser arrays," Optica, vol. 4, no. 3, pp. 323–329, 2017.
- [24] W. Liu et al., "An integrated parity-time symmetric wavelength-tunable single-mode microring laser," Nature Commun., vol. 8, May 2017, Art. no. 15389.
- [25] R. Yao, C.-S. Lee, V. Podolskiy, and W. Guo, "Electrically injected parity time-symmetric single transverse-mode lasers," *Laser Photon. Rev.*, vol. 13, no. 1, 2019, Art. no. 1800154.
- [26] Z. J. Wong et al., "Lasing and anti-lasing in a single cavity," Nature Photon., vol. 10, pp. 796–801, Dec. 2016.
- [27] B. Zhen et al., "Spawning rings of exceptional points out of Dirac cones," Nature, vol. 525, no. 7569, pp. 354–358, Sep. 2015.
- [28] J. Doppler et al., "Dynamically encircling an exceptional point for asymmetric mode switching," *Nature*, vol. 537, no. 7618, pp. 76–79, 2016.
- [29] H. Xu, D. Mason, L. Jiang, and J. G. E. Harris, "Topological energy transfer in an optomechanical system with exceptional points," *Nature*, vol. 537, pp. 80–83, Sep. 2016.
- [30] J. Wiersig, "Enhancing the sensitivity of frequency and energy splitting detection by using exceptional points: Application to microcavity sensors for single-particle detection," Phys. Rev. Lett., vol. 112, no. 20. 2014. Art. no. 203901.
- [31] H. Hodaei et al., "Enhanced sensitivity at

- higher-order exceptional points," Nature, vol. 548, pp. 187-191, Aug. 2017.
- W. Chen, Ş. K. Özdemir, G. Zhao, J. Wiersig, and L. Yang, "Exceptional points enhance sensing in an optical microcavity," Nature, vol. 548, pp. 192-196, Aug. 2017.
- [33] R. El-Ganainy, K. G. Makris, M. Khajavikhan, Z. H. Musslimani, S. Rotter, and D. N. Christodoulides, "Non-Hermitian physics and PT symmetry," Nature Phys., vol. 14, no. 1, p. 11. 2018.
- [34] L. Feng, R. El-Ganainy, and L. Ge, "Non-Hermitian
- photonics based on parity-time symmetry," Nature
- Photon., vol. 11, pp. 752–762, Dec. 2017.
 [35] M.-A. Miri and A. Alù, "Exceptional points in optics and photonics," Science, vol. 363, p. 7709, Jan. 2019.
- [36] S. K. Özdemir, S. Rotter, F. Nori, and L. Yang, "Parity-time symmetry and exceptional points in photonics," Nature Mater., vol. 18, pp. 783-798, Apr. 2019.
- K. J. Vahala, "Optical microcavities," Nature, vol. 424, no. 6950, pp. 839-846, Aug. 2003.
- [38] A. U. Hassan, H. Hodaei, M. A. Miri, M.
- Khajavikhan, and D. N. Christodoulides, "Nonlinear reversal of the PT-symmetric phase transition in a system of coupled semiconductor microring resonators," Phys. Rev. A, Gen. Phys., vol. 92, Dec. 2015, Art. no. 063807.
- [39] H. Hodaei et al., "Design considerations for single-mode microring lasers using parity-time-symmetry," IEEE J. Sel. Topics Quantum Electron., vol. 22, no. 5, pp. 12–18, Mar. 2016. [40] J. Ren et al., "Unidirectional light emission in
- PT-symmetric microring lasers," Opt. Express, vol. 26, no. 21, pp. 27153-27160, 2018.

ABOUT THE AUTHORS

William E. Hayenga received the B.Sc. degree in physics from Iowa State University, Ames, IA, USA, in 2012, the M.Sc. degree from the University of Central Florida, Orlando, FL, USA, in 2016, and the Ph.D. degree from CREOL, The College of Optics and Photonics, University of Central Florida, in 2018.



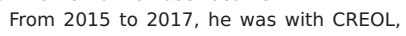


Midya Parto received the B.Sc. and M.Sc. degrees in electrical engineering from the University of Tehran, Tehran, Iran, in 2011 and 2014, respectively, and the M.Sc. degree in optics and photonics from CREOL, The College of Optics and Photonics, University of Central Florida, Orlando, FL, USA, in 2016. He is currently working toward the Ph.D. degree at the Nonlinear Waves Group, CREOL, University of Central Florida.



His current research interests include novel on-chip semiconductor lasers, active topological photonics, and multicore optical fiber structures.

Hipolito Garcia-Gracia received the B.Sc. and Ph.D. degrees from the Tecnologico de Monterrey, Monterrey, Mexico, in 2006 and 2012, respectively. His Ph.D. degree focused on elliptic quantum billiards, generation of quasi-nondifracting optical patterns, and novel methods for calculating orbital angular momentum of laser beams.



The College of Optics and Photonics, University of Central Florida, Orlando, FL, USA, as a Postdoctoral Researcher, where he was involved in the design and fabrication of metallic nanolasers and parity-time (PT)-symmetric double-ring lasers. He has authored and coauthored more than 20 publications in peer-reviewed journals and conferences.

Hossein Hodaei received the B.Sc. degree from the Isfahan University of Technology, Isfahan, Iran, in 2011, the M.Sc. degree in electrical engineering from the Sharif University of Technology, Tehran, Iran, in 2013, and the Ph.D. degree from CREOL, The College of Optics and Photonics, University of Central Florida, Orlando, FL, USA, in 2017.



He is currently with Infinera Corporation, Sunnyvale, CA, USA. His current research interests include paritytime symmetry, novel semiconductor lasers, and non-Hermitian optics.

Enrique Sanchez Cristobal received the B.Sc. degree in electronics from the Meritorious Autonomous University of Puebla, Puebla, Mexico, in 2013, and the M.Sc. degree from the National Institute of Astrophysics, Optics and Electronics, Puebla, in 2015. He is currently working toward the Ph.D. degree at CREOL. The College of Optics and Photonics, University of Central Florida, Orlando, FL, USA.



Patrick LiKamWa received the Ph.D. degree in electrical engineering from the University of Sheffield, Sheffield, U.K., in 1987.

He is currently a Professor of optics and photonics with a joint secondary appointment with the Department of Electrical and Computer Engineering, University of Central Florida, Orlando, FL, USA. His current



research interests include the design, fabrication, and testing of novel optoelectronic devices using III-V multiquantum well semiconductors and the integration of high-speed optical and optoelectronic devices to form monolithic and hybrid integrated optical circuits for high-speed optical networks and optical sensing applications.

Demetrios N. Christodoulides received the Ph.D. degree from Johns Hopkins University, Baltimore, MD, USA, in 1986.

He joined Bellcore, Murray Hill, NY, USA, as a Postdoctoral Fellow for two years. From 1988 to 2002, he was with the Faculty of the Department of Electrical Engineering, Lehigh University, Bethlehem, PA, USA. He is currently the Cobb Family Endowed Chair



and the Pegasus Professor of optics with CREOL, The College of Optics and Photonics, University of Central Florida, Orlando, FL, USA. He has authored and coauthored more than 380 papers. His current research interests include linear and nonlinear optical beam interactions, synthetic optical materials, optical solitons, and quantum electronics. His research initiated new innovation within the field, including the discovery of optical discrete solitons, Bragg and vector solitons in fibers, nonlinear surface waves, and the discovery of self-accelerating optical (Airy) beams.

Dr. Christodoulides is a fellow of the Optical Society of America (OSA) and the American Physical Society. He was a recipient of the OSA 2011 R.W. Wood Prize and of the 2018 Max Born Award of OSA.

Mercedeh Khajavikhan received the Ph.D. degree in electrical engineering from the University of Minnesota, Minneapolis, MN, USA, in 2009.

She subsequently joined the University of California at San Diego, San Diego, CA, USA, as a Postdoctoral Researcher, where she was involved in the design and development of nanolasers, plasmonic devices, and silicon



photonics components, for three years. In 2012, she joined as a Faculty Member with CREOL, The College of Optics and Photonics, University of Central Florida, Orlando, FL, USA, for seven years. In 2019, she started as an Associate Professor with the Electrical and Computer Engineering Department, University of Southern California, Los Angeles, CA, USA. Her current research interests include exploring novel phenomena in active photonic systems and realization of new devices based on them.